Supplementary Information

High-temperature All-organic Energy Storage Dielectric with Performance of Self-adjusting Electric Field Distribution

Guang Liu,[ab] Yu Feng,[*ab] Tiandong Zhang,[ab] Changhai Zhang,[ab] Qingguo Chi,[*ab] Yongquan Zhang,[ab] Yue Zhang,[ab] Qingquan Lei[ab]

[a] *Key Laboratory of Engineering Dielectrics and Its Application, Ministry of Education, Harbin University of Science and Technology, Harbin 150080, PR China*

[b] *School of Electrical and Electronic Engineering, Harbin University of Science and Technology, Harbin 150080, PR China*

[*] *Corresponding author: E-mail: fengyu@hrbust.edu.cn (Yu Feng), qgchi@hotmail.com (Qingguo Chi).*

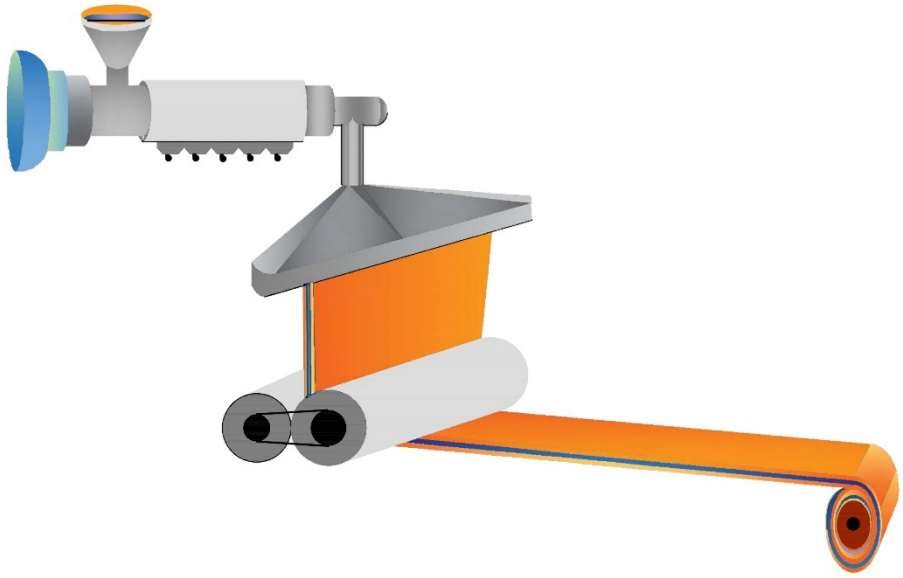

Fig. S1. Simplified flow chart of industrialized production of sandwich structure composite dielectric.

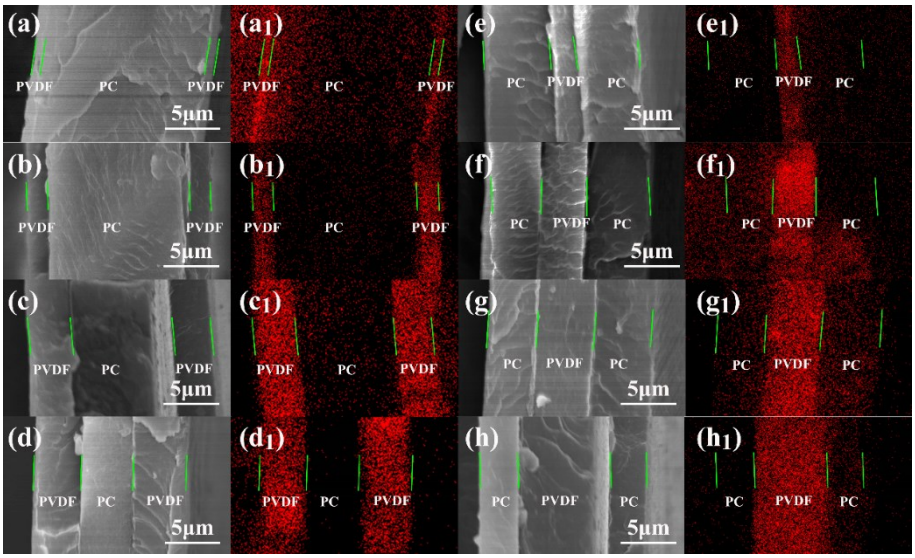

Fig. S2. SEM spectrum of composite dielectric and the corresponding F element mapping. (a) FCF-1; (b) FCF-2; (c) FCF-3; (d) FCF-4; (e) CFC-2; (f) CFC-4; (g) CFC-6; (h) CFC-8.

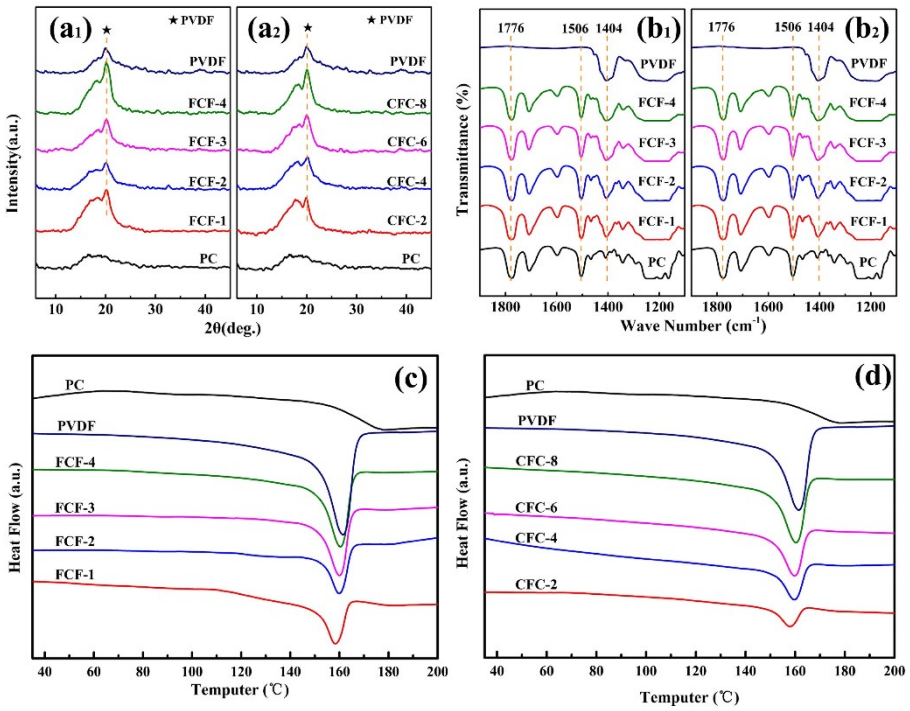

Fig. S3. Structural characteristics of composite dielectrics. XRD (a); FT-IR (b); DSC of FCF structure (c) and CFC structure (d).

Figures S3(a_1)-(a_2) are the XRD patterns of the FCF and CFC structure composite dielectrics. It can be seen from the figure that the two diffraction peaks of the composite dielectric correspond to the characteristic diffraction peaks of PC and PVDF respectively, and there is no new diffraction peak generated. This shows that the two types of composite dielectrics prepared are the physical combination of PC and PVDF without new phase generation. In addition, it can be seen from the figure that the prepared dielectric film has a bulge at a 2θ of about 16°, which corresponds to amorphous PC[1-2]. As the thickness of the PC layer decreases, the bulge becomes less noticeable. As the PVDF thickness in the composite dielectric gradually increases, the corresponding PVDF characteristic peak at 20° gradually increases, which is due to the gradual increase in the PVDF content in the composite dielectric[3]. Figure S3(b_1)-(b_2) are the FT-IR of FCF and CFC structure composite dielectrics respectively. It can also be seen that as the thickness of the PVDF layer increases, the absorption peak area significant increased corresponding to the PVDF at a wavelength of 1404 cm^{-1}[4-5]. There are two strong transmission peaks at 1506 cm^{-1} and 1770 cm^{-1}, which are derived from the aromatic ring of PC and C=O tensile vibration respectively[6-7].

In order to understand the influence of different PVDF and PC content on the thermal performance of the composite dielectric, the DSC test on the composite dielectric was conducted, and the results are shown in Figure S3(c)-(d). It can be seen that as the content of PC increases, the glass transition temperature T_g of the composite dielectric gradually increases, that is because PC has excellent temperature tolerance. The glass transition temperature of composite dielectrics is higher than that of PVDF (~145℃). This is due to the existence of PC effectively improves the heat resistance of composites. On the whole, the composite dielectrics of FCF-1 and CFC-2 have higher glass transition temperature (~150℃), which means that these two composite dielectrics have better thermal stability, and the thermal stability of CFC-2 is even better, compared with FCF-1. This is

mainly because the outer layer of PC, which reduces the free volume of the composite dielectric and improves the thermal stability of the composite dielectric[8-9]. Good heat resistance provides a strong guarantee for the application of composite dielectrics in high temperature environments.

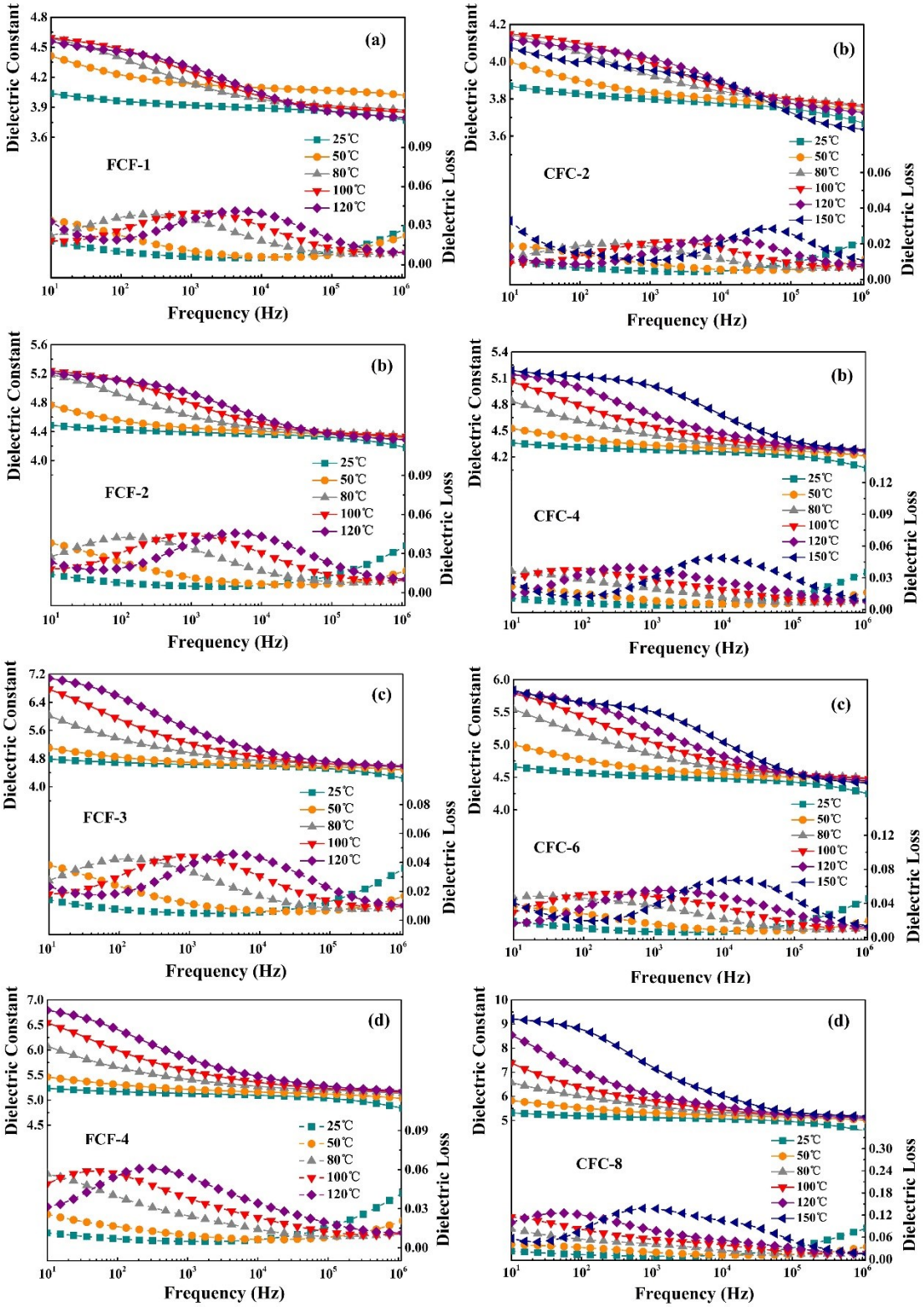

Fig. S4. Broadband dielectric for composite dielectrics at different temperatures.

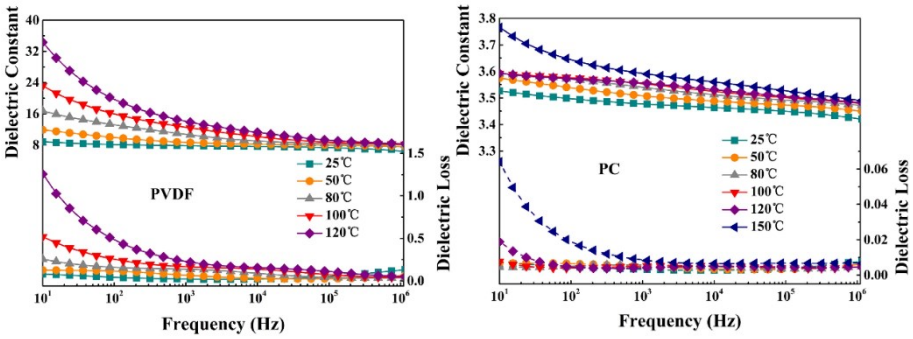

Fig. S5. Broadband dielectric for PVDF and PC at different temperatures.

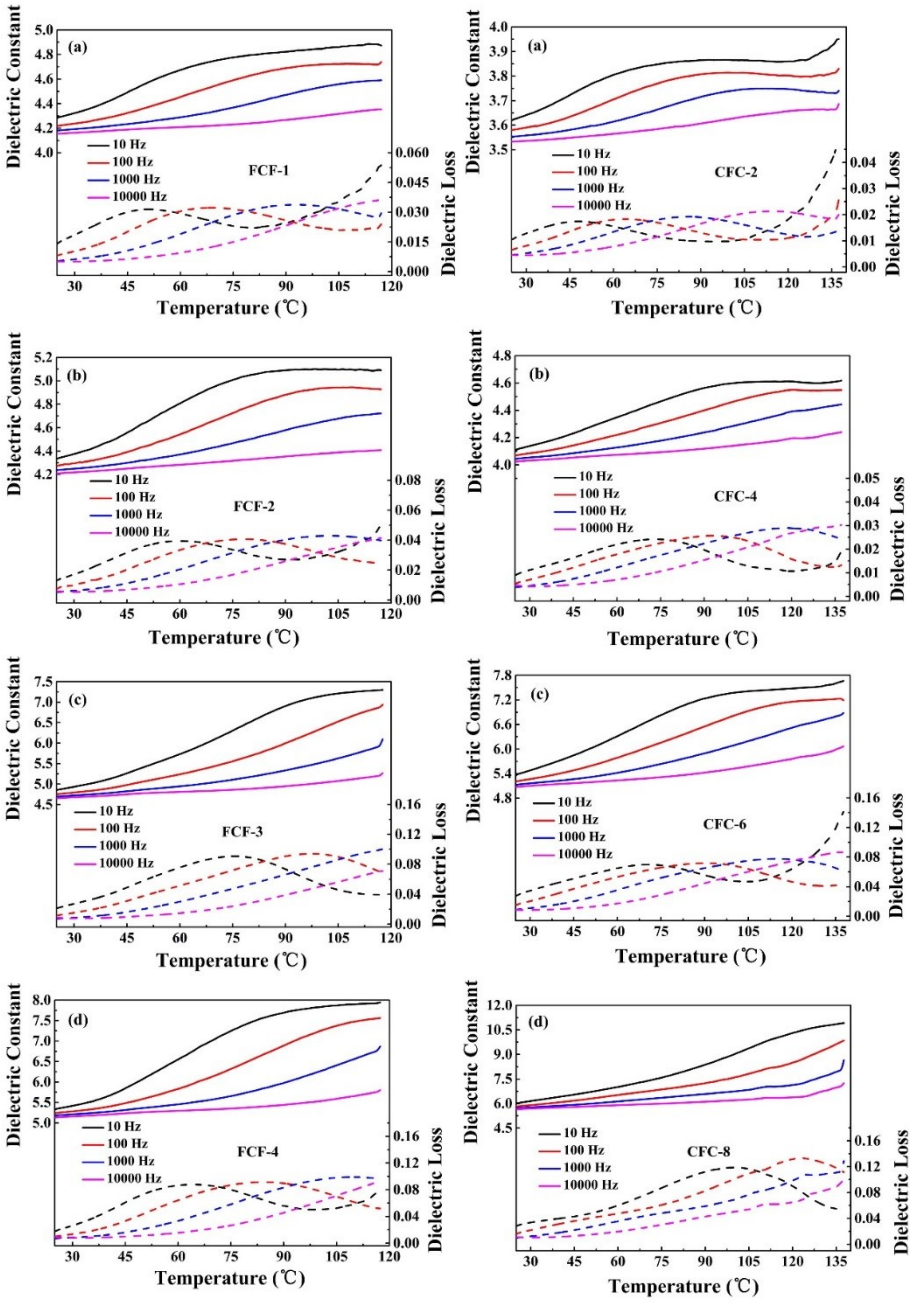

Fig. S6. The relationship between the dielectric constant of the composite dielectric and the temperature.

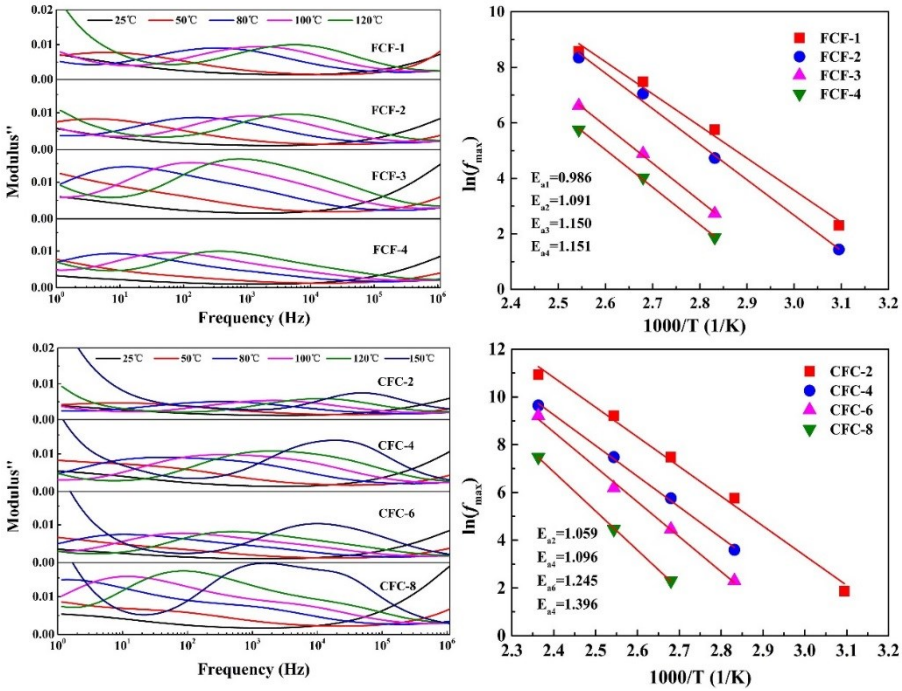

Fig. S7. Variation of imaginary part of dielectric modulus of composite dielectric with Temperature.

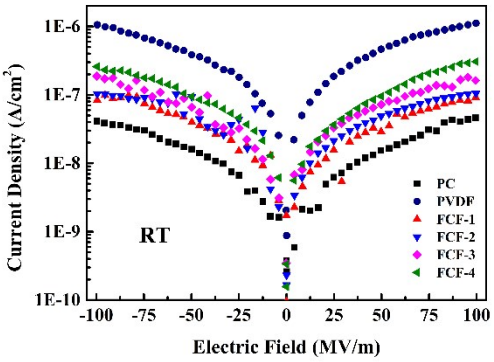
Current Density (A/cm²)
1E-6
1E-7
1E-8
1E-9
1E-10
-100 -75 -50 -25 0 25 50 75 100
Electric Field (MV/m)
RT
PC
PVDF
FCF-1
FCF-2
FCF-3
FCF-4

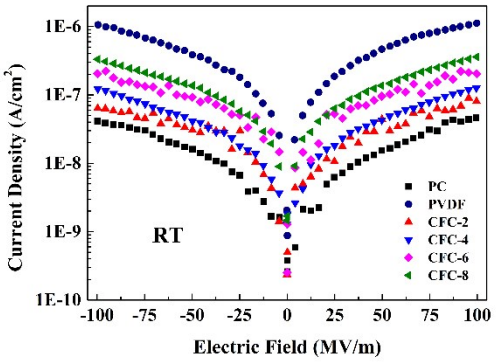
Current Density (A/cm²)
1E-6
1E-7
1E-8
1E-9
1E-10
-100 -75 -50 -25 0 25 50 75 100
Electric Field (MV/m)
RT
PC
PVDF
CFC-2
CFC-4
CFC-6
CFC-8

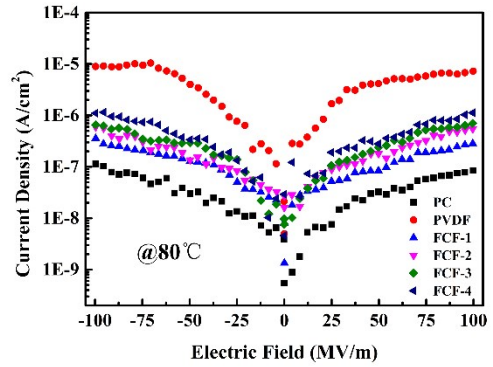
Current Density (A/cm²)
1E-4
1E-5
1E-6
1E-7
1E-8
1E-9
-100 -75 -50 -25 0 25 50 75 100
Electric Field (MV/m)
@80℃
PC
PVDF
FCF-1
FCF-2
FCF-3
FCF-4

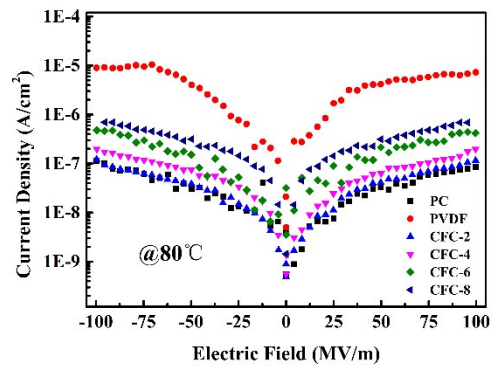
Current Density (A/cm²)
1E-4
1E-5
1E-6
1E-7
1E-8
1E-9
-100 -75 -50 -25 0 25 50 75 100
Electric Field (MV/m)
@80℃
PC
PVDF
CFC-2
CFC-4
CFC-6
CFC-8

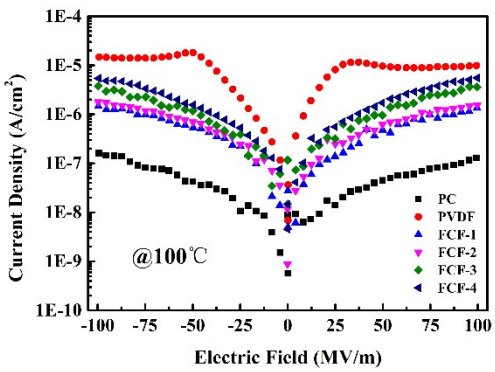
Current Density (A/cm²)
1E-4
1E-5
1E-6
1E-7
1E-8
1E-9
1E-10
-100 -75 -50 -25 0 25 50 75 100
Electric Field (MV/m)
@100℃
PC
PVDF
FCF-1
FCF-2
FCF-3
FCF-4

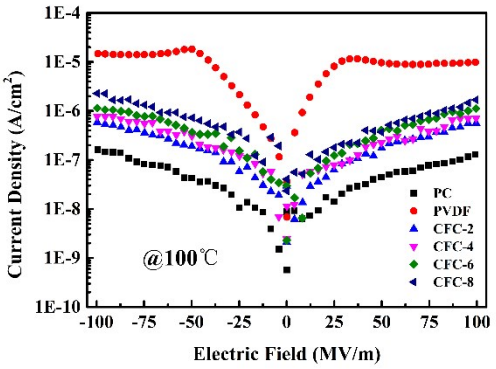
Current Density (A/cm²)
1E-4
1E-5
1E-6
1E-7
1E-8
1E-9
1E-10
-100 -75 -50 -25 0 25 50 75 100
Electric Field (MV/m)
@100℃
PC
PVDF
CFC-2
CFC-4
CFC-6
CFC-8

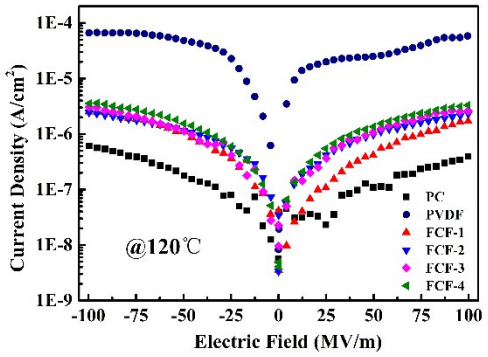
Current Density (A/cm²)
1E-4
1E-5
1E-6
1E-7
1E-8
1E-9
-100 -75 -50 -25 0 25 50 75 100
Electric Field (MV/m)
@120℃
PC
PVDF
FCF-1
FCF-2
FCF-3
FCF-4

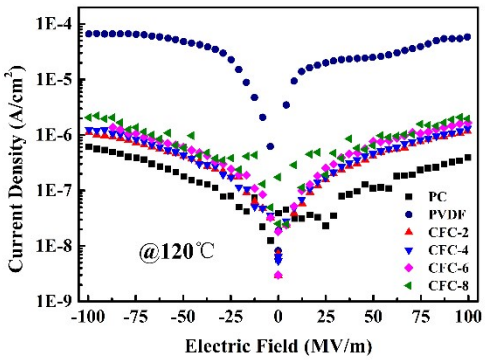
Current Density (A/cm²)
1E-4
1E-5
1E-6
1E-7
1E-8
1E-9
-100 -75 -50 -25 0 25 50 75 100
Electric Field (MV/m)
@120℃
PC
PVDF
CFC-2
CFC-4
CFC-6
CFC-8

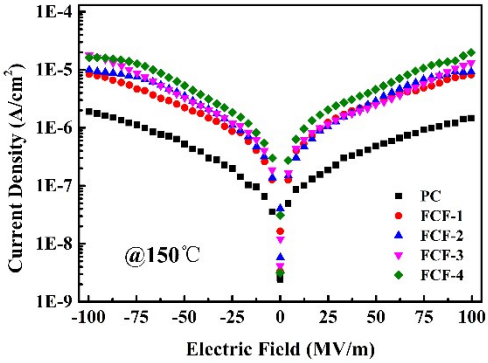
Current Density (A/cm²)
1E-4
1E-5
1E-6
1E-7
1E-8
1E-9
-100 -75 -50 -25 0 25 50 75 100
Electric Field (MV/m)
@150℃
PC
FCF-1
FCF-2
FCF-3
FCF-4

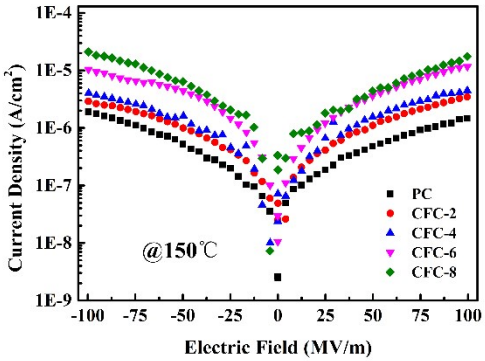
Current Density (A/cm²)
1E-4
1E-5
1E-6
1E-7
1E-8
1E-9
-100 -75 -50 -25 0 25 50 75 100
Electric Field (MV/m)
@150℃
PC
CFC-2
CFC-4
CFC-6
CFC-8

Fig. S8. Current density of composite dielectric at different temperatures.

In order to analyze the insulation performance of the material more comprehensively, we calculated the thermal activation energy of several composite dielectrics prepared, and further explained the influences of relative position and different thickness of the PC layer and the PVDF layer on the thermal activation energy of the composite dielectric. The calculation result is shown in Fig. S9.

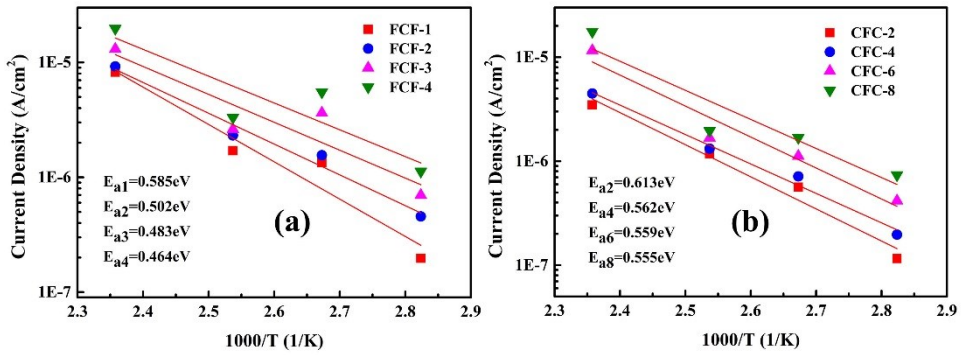

Fig. S9. The relationship between current density and the reciprocal of temperature in an electric field of 100 MV/m

The figure shows the thermal activation energy of several composite dielectrics. Through comparison, it can be found that in the same structure, as the thickness of the PVDF layer gradually increases, the thermal activation energy of the composite dielectric gradually decreases. This shows that when an electric field is applied, the thicker the PVDF layer is, the easier the thermal activation process is to occur, which also reflects the worse the insulation performance.

In addition, by comparing the two structures, it can be found that when the total thickness of the PVDF layer is the same, the activation energy of the composite dielectric with the PC layer on the outside is greater than the activation energy of the PVDF on the outside. This shows that it is more difficult to induce thermal-activation process in CFC structure dielectrics, which means that they has better insulation.

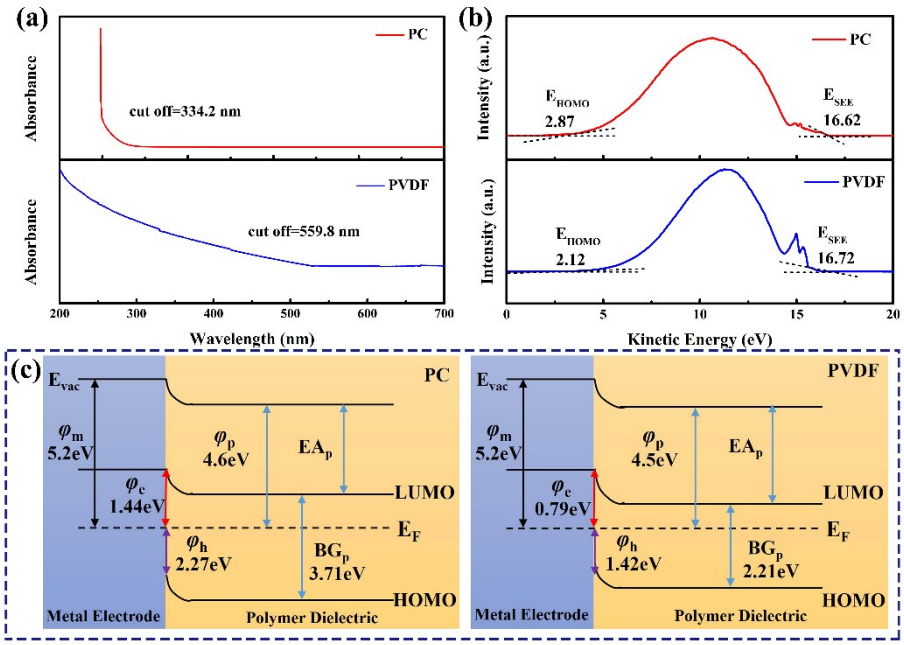

Fig. S10 UV-Vis spectrum of PC and PVDF polymers (a); Ultraviolet photoelectron spectra of PC and PVDF polymers (b); Band diagrams at the electrode/dielectric interface of Au/PC and Au/PVDF (c).

Figure S10(a) shows the Ultraviolet–visible spectroscopy (UV-Vis) of the two materials, according to the test results, the band gap of the two materials can be calculated. The band gap of PC is 3.71eV, and the band gap width of PVDF is 2.21eV

Figure S10(a) shows the Ultroviolet Photoelectron Spectrometer (UPS) spectrum, in the right side of the UPS spectrum of insulation dielectrics, the maximum kinetic energy($E_{k,\,max}$), correspond to the excitation from the HOMO level. The ionization potential (IP) of HOMO can be obtained by

$$IP_{\mathrm{HOMO}} = h\upsilon - (E_{\mathrm{SEE}} - E_{\mathrm{HOMO}})$$

With the obtained ionization potential (IP), the position of the HOMO level can be determined. The position of the LUMO level can be further deduced by the band gap for polymer, respectively to the HOMO level. With the known work function (5.2 eV) of Au, the potential barrier for electrons (ϕe) and holes (ϕh) can be calculated[10-11].

Figure S10(c) is the band diagram. E_{vac} is the vacuum energy level, E_F is the Fermi energy level, LUMO is the lowest unoccupied molecular orbital energy level, HOMO is the highest occupied molecular orbital energy level, ϕ_e is the potential barrier for electrons, and ϕ_h is the potential barrier for holes. The vacuum energy level is called the free electron energy level. When the electron reaches the vacuum energy level, it is completely free of the nucleus. When the temperature is absolute zero, the highest energy level filled with electrons in the energy band of solid is the Fermi level, which is expressed by EFermi. The Fermi level is usually used as the reference level. The difference between the vacuum level and the Fermi level is the work function of the sample.

It can be seen from the figure that the band gap of PC is much larger than that of PVDF, which shows that PC has better insulation. In addition, the ϕ_e and ϕ_h of PC are also much larger than PVDF, which shows that PC can effectively inhibit the injection of carriers on the outside, so the composite

medium of CFC structure has better insulation, especially CFC-1

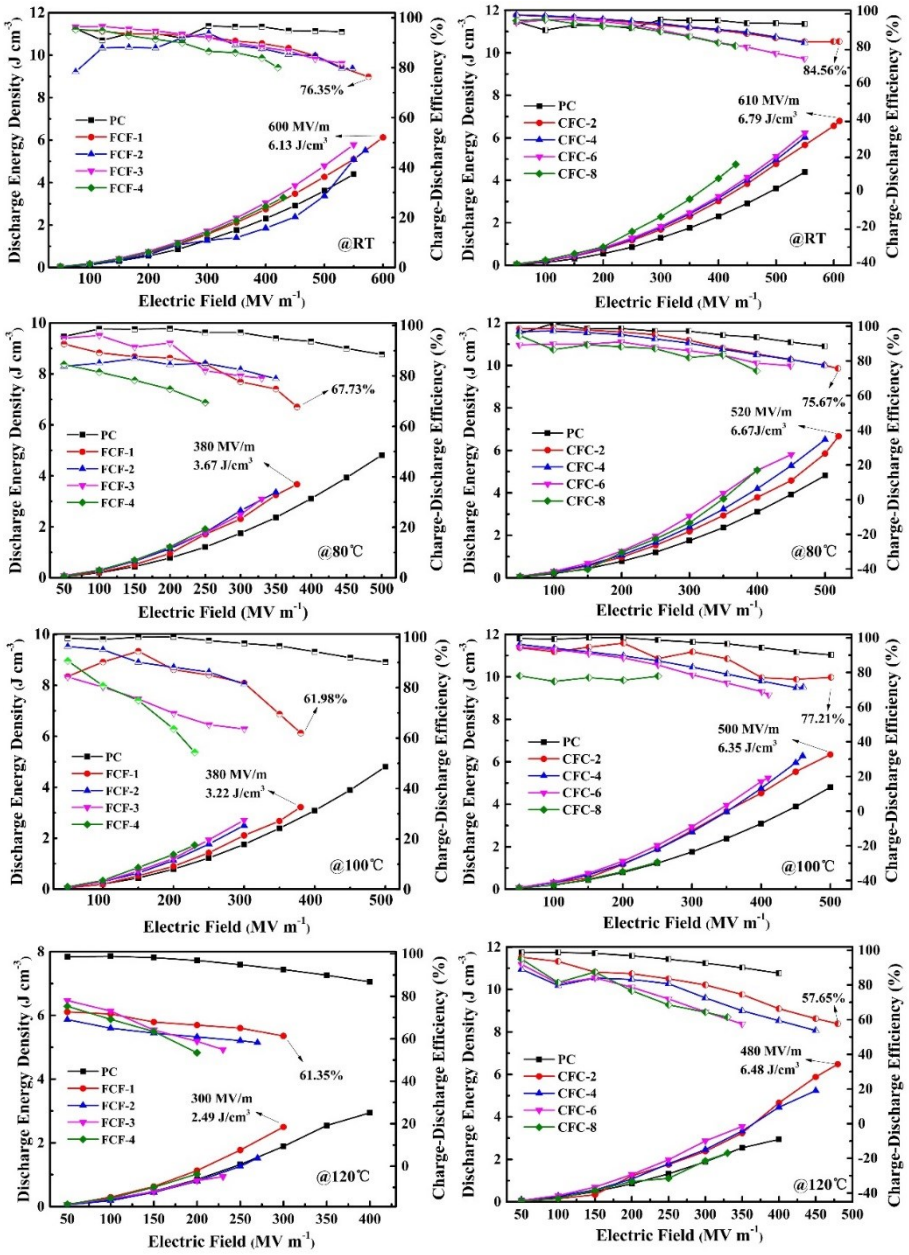

Fig. S11. Energy storage characteristics of composite dielectrics at different temperatures.

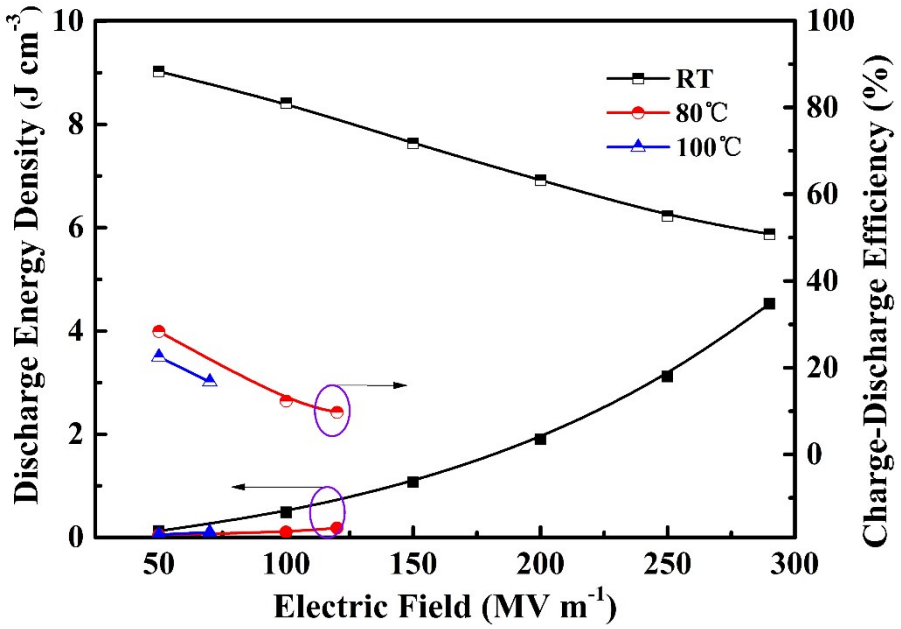

Fig. S12. Energy storage characteristics of PVDF at different temperatures.

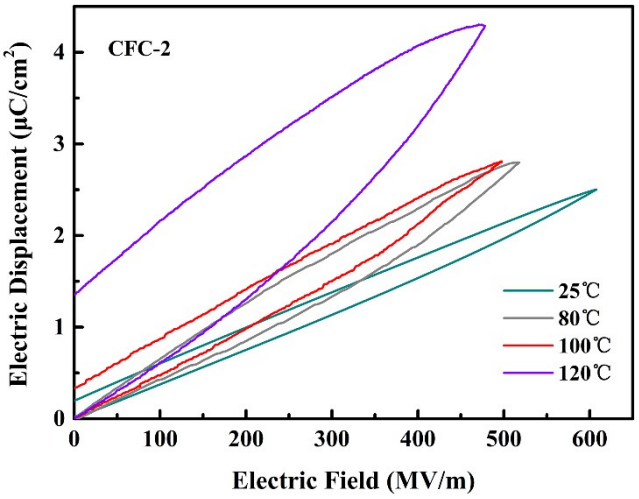

Fig. S13. The electric field-electric displacement curve of CFC-2 under the maximum electric field at different temperatures.

It can be seen from the figure that as the temperature increases, the maximum electric field that the dielectric can withstand gradually decreases, and its charge-discharge efficiency also gradually decreases, especially at 120°C. Its charge-discharge efficiency is the lowest. This is mainly related to the increase in current density caused by high-temperature download current injection, which ultimately leads to serious deterioration of its insulation performance.

As the temperature increases, carrier injection increases, which leads to an increase in the

current density inside the dielectric, which increases the loss and reduces the charge and discharge efficiency. Under an electric field of 100MV/m, the current density of CFC-2 is 5.6E-7 A/cm2 at 100 degrees Celsius, and the current density of CFC-2 is 1.2E-6 A/cm2 at 120 degrees Celsius. The large current density is also It means that its electrical conductivity increases and insulation performance decreases. At 100°C, the electrical conductivity of CFC-2 is 5.6E-11S/m, while at 120°C, its electrical conductivity is 1.2E-10, which is 2.14 times that at 100°C. Taken together, the increase in the electrical conductivity of the composite dielectric at 120°C leads to an increase in its loss, so its capacitance performance is seriously deteriorated.

Related content has been added to the supporting information.

References

[1] P. K. Sain, R. K. Goyal, Y. V. S. S. Prasad and A. K. Bhargava, *J. Electron. Mater.*, 2017, **46**, 458-466.

[2] D. J. Silva, M. T. Escote, S. A. Cruz, D. F. Simiao, A. Zenatti, M. S. Curvello, *Polym. Composite.*, 2018, **39**, E780-E790.

[3] C. Chen, C. H. Zhang, T. D. Zhang, Y. Feng, Y. Q. Zhang, Q. G. Chi, X. Wang and Q. Q. Lei, *Compos. Part B-Eng.*, 2020, **199**, 108312.

[4] P. Yadav, T. D. Raju and S. Badhulika, *ACS Appl. Electron. Mater.*, 2020, **2**, 1970-1980.

[5] S. B. Ye, C. Cheng, X. M. Chen, X. L. Chen, J. Y Shao, J. Zhang, H. W. Hu, H. M. Tian, X. M. Li, L. Ma and W. B. Jia, *Nano Energy*, 2019, **60**, 701-714.

[6] J. W. Lee, J. H. Heo, B. Lee, H. H. Cho, T. Kim and J. H. Lee, *J. Mater. Sci.-Mater. El.*, 2019, **30**, 17773-17779.

[7] S. Yeo, W. J. Cho, D. S. Kim, C. Y. Lee, Y. S. Hwang, J. K. Suk, C. Kim and J. M. Ha, *RSC Adv.*, 2020, **10**, 28603-28607.

[8] M. A. Marwat, W. G. Ma, P. Y. Fan, H. Elahi, C. Samart, B. Nan, H. Tan, D. Salamon, B. H. Ye and H. B. Zhang, *Energy Storage Mater.*, 2020, **31**, 492-504.

[9] Q. Y. Zhang, X. Chen, T. Zhang and Q. M. Zhang, *Nano Energy*, 2019, **64**, 103916.

[10] Y. S. Li, S. Cheng, S. J. Wang, C. Yuan, Z. Luo, Y. J. Zhu, J. Hu, J. L. He and Q. Li, *Compos. Sci. Technol.*, 2021, **202**, 108594.

[11] Y. Zhou, Q. Li, B. Dang, Y. Yang, T. Shao, H. Li, J. Hu, R. Zeng, J. L. He, and Q. Wang, *Adv. Mater.*, 2018, **30**, 1805672.